

Spin-dependent dipole excitation in alkali-metal nanoparticles

Yue Yin, Paul-Antoine Hervieux, Rodolfo A. Jalabert,
Giovanni Manfredi, Emmanuel Maurat, and Dietmar Weinmann
*Institut de Physique et Chimie des Matériaux de Strasbourg, UMR 7504, CNRS-UdS,
23 rue du Loess, BP 43, 67034 Strasbourg Cedex 2, France*

(Dated: February 3, 2022)

We study the spin-dependent electronic excitations in alkali-metal nanoparticles. Using numerical and analytical approaches, we focus on the resonances in the response to spin-dependent dipole fields. In the spin-dipole absorption spectrum for closed-shell systems, we investigate in detail the lowest-energy excitation, the “surface paramagnon” predicted by L. Serra *et al.* [Phys. Rev. A **47**, R1601 (1993)]. We estimate its frequency from simple assumptions for the dynamical magnetization density. In addition, we numerically determine the dynamical magnetization density for all low-energy spin-dipole modes in the spectrum. Those many-body excitations can be traced back to particle-hole excitations of the noninteracting system. Thus, we argue that the spin-dipole modes are not of collective nature. In open-shell systems, the spin-dipole response to an electrical dipole field is found to increase proportionally with the ground-state spin polarization.

PACS numbers: 78.67.Bf, 73.21.-b, 73.22.-f

I. INTRODUCTION

The optical absorption of small metal particles is dominated by the surface plasmon resonance^{1,2,3,4}. In this collective excitation, the center-of-mass of the electrons moves back and forth with respect to the positive background leading to an oscillating charge dipole. Pump-probe experiments using femtosecond laser pulses have been widely used to study the relaxation of these excitations^{5,6}. Within the surface plasmon excitation all the electrons oscillate in phase, irrespective of their spin. Thus, its study only yields information on the charge dynamics. In order to address the spin dynamics of nano-objects, time-resolved magneto-optical Kerr effect measurements have been performed recently, yielding the full trajectory of the magnetization in real space for optically excited superparamagnetic nanoparticles⁷.

A substantial interest in the theoretical description of spin dynamics in nano-objects was aroused by the work of Serra *et al.*⁸, who found that a strong peak in the spin dipole absorption spectrum of alkaline nanoparticles exhausts a large fraction of the energy-weighted sum rule and drew the conclusion that this peak corresponds to a collective spin mode. In this excitation named “surface paramagnon”, the spin degree of freedom appears in a crucial manner. While the surface plasmon can be excited by a dipole electric field, the surface paramagnon results when an excitation acts differently for spin up and spin down electrons. Such a field can be realized experimentally through the magnetic field component of electromagnetic waves having a wavelength considerably longer than the size of the system⁹.

For the case of spherically symmetric systems with zero total spin, in the spin-dipole mode the center-of-mass of the electron system does not move. Therefore, such an excitation does not couple to an electric field in closed-shell systems. Since transitions induced by electric dipole fields are the dominant mechanism, the sur-

face paramagnon is difficult to observe in the optical absorption spectrum of such nanoparticles. However, for nanoparticles with no spherical symmetry and/or open-shell electronic systems, the spin dipole couples to electric dipole fields^{10,11,12}. For relatively small systems, it has been concluded from calculations of the time-evolution of strong excitations that the coupling between the charge and the spin-modes is not crucially modified when the excitation strength is increased into the non-linear régime¹⁰. In systems that lack spherical symmetry scissor modes exist which can also be coupled to the spin-modes¹³.

The difficulty to detect the spin-dipole mode in rotationally invariant nano-objects becomes less restrictive when one studies semiconductor quantum dots instead of metallic nanoparticles. For the typical sizes and electronic densities of quantum dots the energies of the charge and spin dipole excitations are of the order of a few meV. Therefore Raman scattering of visible light can be used (with selection rules depending on the polarization geometry¹⁴) to detect and study both kinds of excitations¹⁵. Finally, the strong electronic confinement of disc-shaped quantum dots in semiconductor heterostructures results in very sharp resonances for dipolar excitations. The enhanced damping of the lowest spin-dipole mode in the presence of a weak magnetic field that splits the single-particle excitations has been taken as an indication of the collective character of the lowest spin-dipole mode¹⁵.

The availability of experimental data has motivated theoretical work on the charge and spin density excitations in semiconductor few-electron quantum dots (see for example Ref. 16). In particular, the induced magnetization density has been studied⁹ and a correspondence between the spin-dipole modes and single-particle excitations has been observed numerically¹⁷. The small deviation of the spin density resonance energies from single-particle excitation energies has been explained by the

absence of long-range Coulomb interaction terms in the energy of the spin modes. In addition, the excitation energies have been studied using the Quantum Monte Carlo technique¹⁸ and within a semiclassical approach for the time-dependent charge and spin density oscillations¹⁹.

In this work, we use analytical (mean-field) and numerical time-dependent local spin-density approximation (TDLSDA) approaches to study in detail the physics of the spin-dipole modes in alkali-metal particles. We address the important questions related to the specificity of the lowest frequency resonance as compared with the other excitations by identifying the modes with the corresponding dynamical magnetization densities.

By studying the evolution of the spin modes with the interaction we provide clear-cut arguments in the discussion over the collective *versus* single-particle nature of the surface paramagnon. In addition we obtain the size scaling of the lowest resonance frequency and relate it with spill-out effects. In the case of open-shell systems we analyze the nature of the different spin-dipole excitations and the relationship with the charge modes.

While our numerical results are worked out for the case of alkaline metal nanoparticles, most of our general conclusions hold for a broad class of nanosystems, including semiconductor quantum dots.

The paper is organized as follows. In Sec. II, we describe the model for the electron dynamics in metal nanoparticles and the numerical method we employ. We also present the computed spin-dipole absorption spectrum and the corresponding dynamical magnetization density for a typical example of a closed-shell system. In Sec. III, we use a phenomenological approach to describe the energetically lowest spin dipole excitation and derive results for its frequency based on plausible assumptions on the dynamical magnetization density. We compare the numerically obtained frequencies with the phenomenological ones resulting from increasingly accurate descriptions of the electronic dynamics. In Sec. IV, we present numerical results for the full absorption cross section in the frequency regime below the surface plasmon frequency. We follow the evolution of the absorption spectrum with the strength of electron-electron interactions and find a one-to-one correspondence of the spin-dipole modes with the particle-hole excitations. In Sec. V, we study open shell clusters and discuss the possibility to observe the spin-dipole modes in the electric dipole absorption spectrum. We provide our conclusions in Sec. VI. In the appendices we present the details of our LSDA parametrization and the calculations for the case of a non-uniform ground-state electron density.

II. NUMERICAL APPROACH TO SPIN-DIPOLE EXCITATIONS

In our study of the electronic excitations of nanoparticles, we restrict ourselves to the electronic degrees of freedom and describe the confining effect of the ionic background by a spherical jellium model with sharp bound-

aries. Such a simplification can be justified for not too small metal particles. Furthermore, we do not consider thermal effects and therefore choose to work at zero temperature.

We start by introducing the formalism underlying the numerical approach to the absorption cross section corresponding to spin-dependent excitations of our model nanoparticles. We follow the formulation of the TDLSDA²⁰ as it is presented in Ref. 16. In this framework the electronic system is described in atomic units ($\hbar = m = e = 4\pi\epsilon_0 = 1$) using the Kohn-Sham equations

$$i\frac{\partial}{\partial t}\phi_k^\sigma(\mathbf{r},t) = \left(-\frac{1}{2}\nabla^2 + V_{\text{eff}}^\sigma(\mathbf{r},t)\right)\phi_k^\sigma(\mathbf{r},t), \quad (1)$$

where ϕ_k^σ is the k^{th} Kohn-Sham wave-function with the quantum number $\sigma = \{\uparrow, \downarrow\}$ describing spin projection onto the $\hat{\mathbf{z}}$ -axis. These wave-functions allow us to define the spin-dependent electron densities

$$n^\sigma(\mathbf{r},t) = \sum_{k \text{ occ}} |\phi_k^\sigma(\mathbf{r},t)|^2, \quad (2)$$

where the sum runs over the single-particle like Kohn-Sham levels k that contribute to the many-body density. The electron density, magnetization density, and spin polarization are obtained from n^σ , respectively, as

$$n = n^\uparrow + n^\downarrow, \quad (3a)$$

$$m = n^\uparrow - n^\downarrow, \quad (3b)$$

$$\xi = m/n. \quad (3c)$$

The effective potential in the Kohn-Sham equations can be written as

$$V_{\text{eff}}^\sigma(\mathbf{r},t) = V_c(\mathbf{r}) + V_H(\mathbf{r},t) + V_{\text{xc}}^\sigma(\mathbf{r},t) + V_{\text{ex}}^\sigma(\mathbf{r},t), \quad (4)$$

where V_c represents the confinement due to the jellium background, V_H is the Hartree potential, V_{xc}^σ is the exchange-correlation potential and V_{ex}^σ stands for the external perturbation. The local character of the approximation is reflected by the choice

$$V_{\text{xc}}^\sigma(\mathbf{r},t) = \frac{\partial}{\partial n^\sigma} (n\epsilon_{\text{xc}}(n^\uparrow, n^\downarrow)) \Big|_{\substack{n^\uparrow=n^\uparrow(\mathbf{r},t) \\ n^\downarrow=n^\downarrow(\mathbf{r},t)}}, \quad (5)$$

where $\epsilon_{\text{xc}}(n^\uparrow, n^\downarrow)$ stands for the exchange-correlation energy density for which we use the parametrization of Perdew and Zunger²¹ reproduced in App. A.

Within linear response theory we write the density changes induced by the external perturbation as

$$\delta n^\sigma(\mathbf{r},\omega) = \sum_{\sigma'} \int d\mathbf{r}' \chi^{\sigma\sigma'}(\mathbf{r},\mathbf{r}',\omega) V_{\text{ex}}^{\sigma'}(\mathbf{r}',\omega), \quad (6)$$

where $V_{\text{ex}}^\sigma(\mathbf{r},\omega)$ is the Fourier transform of the time-dependent external potential, and the response functions $\chi^{\sigma\sigma'}$ obey the Dyson equation

$$\chi^{\sigma\sigma'}(\mathbf{r}, \mathbf{r}', \omega) = \chi_0^{\sigma\sigma'}(\mathbf{r}, \mathbf{r}', \omega) + \alpha_c \sum_{\sigma_1 \sigma_2} \iint d\mathbf{r}_1 d\mathbf{r}_2 \chi_0^{\sigma\sigma_1}(\mathbf{r}, \mathbf{r}_1, \omega) \left[\frac{1}{|\mathbf{r}_1 - \mathbf{r}_2|} + K_{\text{xc}}^{\sigma_1 \sigma_2}(\mathbf{r}_1, \mathbf{r}_2) \right] \chi^{\sigma_2 \sigma'}(\mathbf{r}_2, \mathbf{r}', \omega), \quad (7)$$

where we introduced the parameter $\alpha_c = 1$ which will later allow us to modulate artificially the importance of the electron-electron interactions in model calculations. The kernel of Eq. 7 is given by

$$K_{\text{xc}}^{\sigma_1 \sigma_2}(\mathbf{r}_1, \mathbf{r}_2) = \frac{\partial}{\partial n^{\sigma_2}} (V_{\text{xc}}^{\sigma_1}(n^\uparrow, n^\downarrow)) \Big|_{\substack{n^\uparrow = n^\uparrow(\mathbf{r}_1) \\ n^\downarrow = n^\downarrow(\mathbf{r}_2)}} \delta(\mathbf{r}_1 - \mathbf{r}_2). \quad (8)$$

The non-interacting response function is diagonal in the spin indices and given by the density-density correlator

$$\chi_0^{\sigma\sigma'}(\mathbf{r}, \mathbf{r}', \omega) = \delta_{\sigma, \sigma'} \sum_{jk \text{ occ}} \phi_j^{\sigma*}(\mathbf{r}) \phi_k^\sigma(\mathbf{r}) \phi_k^{\sigma*}(\mathbf{r}') \phi_j^\sigma(\mathbf{r}') \left\{ \frac{1}{\omega - (\varepsilon_k^\sigma - \varepsilon_j^\sigma) + i\eta} - \frac{1}{\omega + (\varepsilon_k^\sigma - \varepsilon_j^\sigma) + i\eta} \right\} \quad (9)$$

which can be expressed in terms of the retarded Green functions^{8,16}. We have chosen the imaginary part in the denominator that ensures the convergence as $\eta = 8 \text{ meV}$ ($= 2.94 \times 10^{-4}$ in atomic units). The robustness of the final result with respect to variations of this parameter has been checked.

Defining the spin-independent part of the external perturbation $V_{\text{ex},n} = (V_{\text{ex}}^\uparrow + V_{\text{ex}}^\downarrow)/2$ and its spin-dependent counterpart $V_{\text{ex},m} = (V_{\text{ex}}^\uparrow - V_{\text{ex}}^\downarrow)/2$, the response of the charge and magnetization densities n and m can be expressed in matrix form as

$$\begin{pmatrix} \delta n(\mathbf{r}, \omega) \\ \delta m(\mathbf{r}, \omega) \end{pmatrix} = \int d\mathbf{r}' \begin{pmatrix} \chi_{nn}(\mathbf{r}, \mathbf{r}', \omega) & \chi_{nm}(\mathbf{r}, \mathbf{r}', \omega) \\ \chi_{mn}(\mathbf{r}, \mathbf{r}', \omega) & \chi_{mm}(\mathbf{r}, \mathbf{r}', \omega) \end{pmatrix} \begin{pmatrix} V_{\text{ex},n}(\mathbf{r}', \omega) \\ V_{\text{ex},m}(\mathbf{r}', \omega) \end{pmatrix}, \quad (10)$$

where the cross-correlations of the charge and spin channels are given by

$$\chi_{nn/nm} = \chi^{\uparrow\uparrow} \pm \chi^{\uparrow\downarrow} + \chi^{\downarrow\uparrow} \pm \chi^{\downarrow\downarrow}, \quad (11a)$$

$$\chi_{mn/mm} = \chi^{\uparrow\uparrow} \pm \chi^{\uparrow\downarrow} - \chi^{\downarrow\uparrow} \mp \chi^{\downarrow\downarrow}. \quad (11b)$$

Electromagnetic radiation with wavelength much larger than the size of the nanoparticles induces dipolar perturbations. Considering monochromatic light with wave-vector $\mathbf{k} = k\hat{\mathbf{x}}$, linear polarization along $\hat{\mathbf{y}}$, and therefore magnetic field along the $\hat{\mathbf{z}}$ -direction, the dipole excitation potentials for charge and spin can be written as

$$V_{\text{ex},n}(\mathbf{r}, t) = F_n y, \quad (12a)$$

$$V_{\text{ex},m}(\mathbf{r}, t) = F_m x, \quad (12b)$$

with the excitation strengths $F_n = -E_{\text{max}} \sin(\omega t)$ and $F_m = g\mu_B E_{\text{max}} k \cos(\omega t)$, the Bohr magneton μ_B , and the gyromagnetic factor g ($g\mu_B = 1$ in atomic units). These dipolar perturbations lead to dipolar charge and spin-density excitations, and the corresponding polarizabilities are given by

$$\alpha_{\text{ab}}(\omega) = \iint d\mathbf{r} d\mathbf{r}' r r' \cos \theta \cos \theta' \chi_{\text{ab}}(\mathbf{r}, \mathbf{r}', \omega), \quad (13)$$

with $\text{ab} = \{\text{nn}, \text{nm}, \text{mn}, \text{mm}\}$. For the simplicity of notations, the polar coordinates (r, θ, φ) are here and henceforth chosen to have the $\hat{\mathbf{z}}$ -axis along the variation of the excitation field. This conventional choice allows us

to treat the charge and spin excitations within the same description, but it is not consistent with the example of electromagnetic radiation presented above.

The experimentally relevant quantities are the dipole absorption cross-sections

$$S_{\text{ab}}(\omega) = \frac{4\pi\omega}{c} \text{Im}[\alpha_{\text{ab}}(\omega)]. \quad (14)$$

For spherically symmetric nanoparticles α and S are diagonal in the channel indices a and b . In this case we will work with $S_n = S_{nn}$ and $S_m = S_{mm}$. The spin-dipole absorption spectrum $S_m(\omega)$ for the closed-shell system Na_{34} ²² is shown in the left panel of Fig. 1. Four peaks are observed in the low-energy range below $0.6\omega_M$, with the Mie frequency $\omega_M = 3.4 \text{ eV}$ which is the classical frequency of the surface plasmon excitation¹. The peak at the lowest frequency, labeled (1) in the figure, displays the strongest absorption cross-section and corresponds to the surface paramagnon described by Serra *et al.*⁸. In section III we derive analytical expressions that accurately describe its frequency and its dependence on the size of the nanoparticle.

The radial part of the magnetization density at resonance is shown in Fig. 1 (right) for the four peaks appearing in the absorption spectrum. The magnetization profile for the lowest frequency peak (1) clearly differs from the profiles corresponding to the higher frequency peaks: it involves considerably stronger magnetization densities than the other peaks and, most importantly, it displays no significant nodes (except at the center of

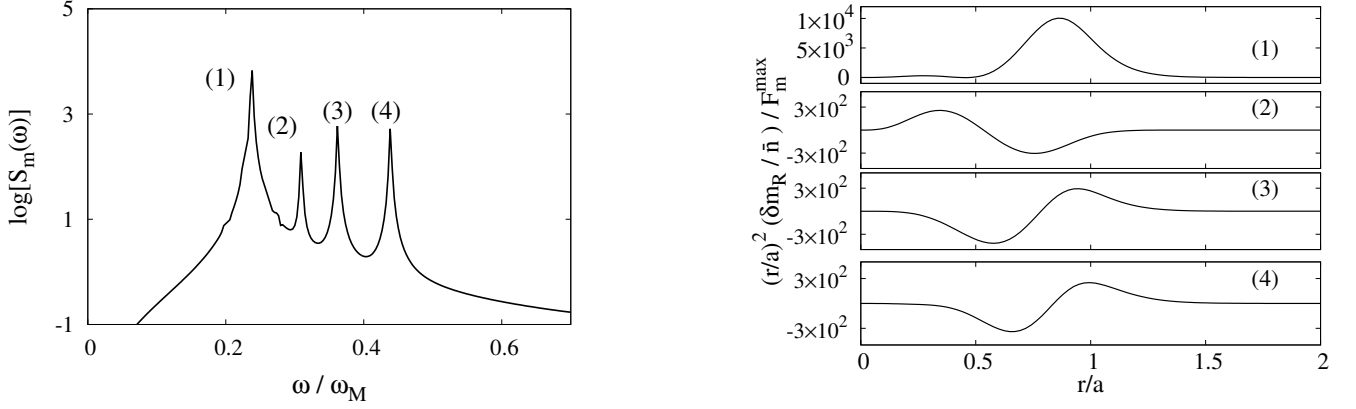


FIG. 1: Left: spin-dipole absorption spectrum for a Na_{34} nanoparticle. The frequencies of the horizontal axis are normalized to the Mie frequency $\omega_M = 3.4 \text{ eV}$ ($= 0.125$ in atomic units). Right: radial part of the magnetization density for each of the resonances identified in the left panel, as a function of the radial coordinate (scaled with the radius a of the particle). The magnetization profile is scaled with the excitation strength, the mean density and the radial coordinate

the nanoparticle), whereas the other peaks are associated to magnetization profiles with richer node structures inside the nanoparticle. For larger systems, even more peaks appear, and the corresponding magnetization profiles show more complicated structures with several nodes. However, the particularly simple structure of the lowest-frequency peak, and its stronger amplitude, persist and thereby point to its special character.

III. PHENOMENOLOGICAL APPROACH TO SPIN-DIPOLE EXCITATIONS

The physics of the spin-dipole excitations obtained in the previous section can be understood through phenomenological models. In particular, we present an estimation of the lowest resonant frequency and compare it with results from TDLSDA calculations.

We consider a spherically symmetric nanoparticle with ground-state equilibrium densities $n_0^\uparrow(\mathbf{r}) = n_0^\downarrow(\mathbf{r})$ and a perturbation in the spin channel such that $\Delta n^\uparrow(\mathbf{r}) = -\Delta n^\downarrow(\mathbf{r})$. The displacements of the center-of-mass of the two spin populations along the $\hat{\mathbf{z}}$ -direction are given by

$$Z^\uparrow = -Z^\downarrow = \frac{1}{N^\uparrow} \int d\mathbf{r} z \Delta n^\uparrow(\mathbf{r}), \quad (15)$$

where $N^\uparrow = N/2$ is the number of spin-up electrons and N the total number of electrons. Since there is no net charge displacement, the Hartree term E_H of Eq. A5 remains unchanged under the perturbation. The changes in the other contributions to the total energy can be calculated from $\Delta n^\uparrow(\mathbf{r})$.

A. Uniform ground-state density

The ground-state equilibrium electron density in a spherical jellium model of radius a with sharp boundaries can be approximated by a uniform distribution

$$n^\uparrow(\mathbf{r}) = n^\downarrow(\mathbf{r}) = \frac{\bar{n}}{2} \Theta(a - r) \quad (16)$$

inside the sphere, where $\bar{n} = 3N/4\pi a^3$ and Θ denotes the Heaviside function. Assuming that the perturbation is a dipolar field, the simplest approximation to describe the low-energy spin excitations of the system is to postulate the tilts

$$\Delta n^\uparrow(\mathbf{r}) = -\Delta n^\downarrow(\mathbf{r}) = \frac{z}{\zeta} \frac{\bar{n}}{2} \Theta(a - r) \quad (17)$$

of the spin densities. The characteristic length ζ describes the magnitude of the excitation. Working in linear response, we restrict ourselves to weak excitations with $\zeta \gg a$ and consider the change in total energy induced by the above density excitations using the energy functionals described in App. A.

The simple form assumed for the spin densities allows us to neglect the change of $E_{K,G}$. To the lowest order in the perturbation the other components of the energy are

modified as

$$\begin{aligned}\Delta E_{K,TF} &= \frac{2\pi^{4/3}}{3^{1/3}} \int d\mathbf{r} \frac{(\Delta n^\uparrow)^2}{\bar{n}^{1/3}} \\ &= \frac{5}{4} \left(\frac{3\pi^2}{2} \right)^{1/3} N^{5/3} \frac{Z^{\uparrow 2}}{a^4},\end{aligned}\quad (18a)$$

$$\begin{aligned}\Delta E_X &= -\frac{2}{(9\pi)^{1/3}} \int d\mathbf{r} \frac{(\Delta n^\uparrow)^2}{\bar{n}^{2/3}} \\ &= -\frac{5}{6} \left(\frac{3}{2\pi} \right)^{2/3} N^{4/3} \frac{Z^{\uparrow 2}}{a^3},\end{aligned}\quad (18b)$$

$$\begin{aligned}\Delta E_C &= \frac{2}{(9\pi)^{1/3}} \int d\mathbf{r} c(\bar{r}_s) \frac{(\Delta n^\uparrow)^2}{\bar{n}^{2/3}} \\ &= \frac{5}{6} \left(\frac{3}{2\pi} \right)^{2/3} c(\bar{r}_s) N^{4/3} \frac{Z^{\uparrow 2}}{a^3}.\end{aligned}\quad (18c)$$

We have defined

$$c(r_s) = \frac{1}{3} \left(\frac{2^{4/3}}{2^{1/3} - 1} \right) \left(\frac{4\pi}{3} \right)^{2/3} r_s [\epsilon^P(r_s) - \epsilon^U(r_s)] \quad (19)$$

with $\epsilon^{P,U}$ given in App. A and $\bar{r}_s = (4\pi\bar{n}/3)^{-1/3}$. The energy increase due to the spin density displacements leads to a restoring force $\mathcal{F} = -\partial E/\partial Z^\uparrow$ and an out-of-phase oscillation of the two spin subsystems with a frequency

$$\begin{aligned}\omega_S &= \sqrt{\frac{2}{N} \frac{\Delta E}{Z^{\uparrow 2}}} \\ &= \frac{\omega_M}{N^{1/3}} \left(\frac{3}{2\pi} \right)^{1/3} \left[\frac{5}{3} \left(\left(\frac{3\pi^2}{2} \right)^{2/3} \frac{1}{\bar{r}_s} - 1 + c(\bar{r}_s) \right) \right]^{1/2}.\end{aligned}\quad (20)$$

We have expressed the result in terms of the classical Mie frequency¹ which can be written as $\omega_M = \sqrt{N/a^3} = (\bar{r}_s)^{-3/2}$.

As compared to the spin dipole, the surface plasmon excitation is of quite different nature since it results from the oscillation of the total charge. The frequency ω_M can be obtained following similar lines as those presented above, but restricting the restoring force to the Hartree contribution. The different nature of the energies involved in each mode results in a higher frequency for the surface plasmon (in the visible part of the spectrum for the case of metal nanoparticles) than for the spin dipole (in the infrared range). Moreover, ω_M is independent of the size of the particle, while ω_S decreases with the number of electrons as $N^{-1/3}$. This power-law scaling has already been obtained in Ref. 23 within sum rule and hydrodynamic approaches. It makes the observation of the surface paramagnon in large particles more difficult.

In Fig. 2 we compare the values of ω_{sd} obtained from the TDLSDA (filled circles) with the estimate ω_S of Eq. 20 (dotted line). For comparison we also show the numerically calculated surface plasmon frequencies ω_{sp} (filled squares), which approach the classical value ω_M for large N and display important oscillations for small N [24].

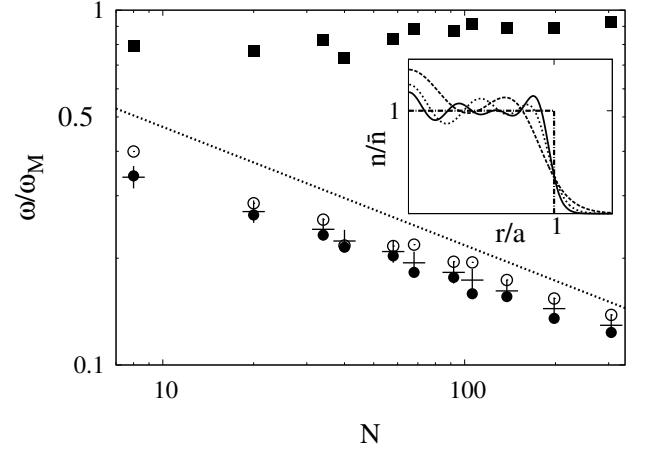


FIG. 2: Size-dependence of the surface paramagnon frequency, together with the surface plasmon frequency ω_{sp} (filled squares). Filled circles represent ω_{sd} obtained from TDLSDA calculations. The dotted line is the estimate ω_S of Eq. 20. The open circles stand for the spill-out corrected Eq. 20, where ω_{sp} is used instead of ω_M in the prefactor. The pluses depict the semi-analytical result of (28) using the magnetization profile arising from Eq. 26. Inset: Radial variation of the ground-state electron density used in Eq. 26, and obtained from static LSDA calculations. The dashed, dotted, and solid lines are for Na_{20} , Na_{106} , and Na_{306} , respectively. \bar{n} is the electron density for bulk Na and the dash-dotted step function corresponds to the uniform ionic jellium.

We can see that the predicted decrease of the spin-dipole frequency as $N^{-1/3}$ is essentially correct. However, Eq. 20 overestimates the actual frequencies. This discrepancy becomes increasingly important when the size a of the nanoparticle diminishes. Two key assumptions in the derivation of (20) become less justified when a gets smaller. On one hand, the spill-out effect due to the extension of the electron wave-functions beyond the jellium sphere lowers the electron density as compared to the bulk value^{3,4} (see Fig. 2, inset). On the other hand, assuming the tilt (17) and not considering density gradients in the energy functional may become problematic.

A simple way to approximately include spill-out effects is to use an electronic density which is slightly lower than \bar{n} . In the case of the surface plasmon, where the numerically obtained frequency ω_{sp} is lower than ω_M , such an approach leads to a reduced frequency $\tilde{\omega}_M = \omega_M \sqrt{1 - N_{out}/N}$, where N_{out} is the number of electrons outside the jellium sphere. However, ω_{sp} is still lower than $\tilde{\omega}_M$, and moreover it exhibits a non-monotonous behavior not accounted for by $\tilde{\omega}_M$ (see Fig. 2 and Ref. 24). Assuming that the effect of spill-out on the spin-dipole frequency is similar to the one on the surface plasmon frequency, it is tempting to substitute ω_M by ω_{sp} in Eq. 20. As shown in Fig. 2, such an approach (circles) considerably improves the estimation of ω_{sd} .

B. Non-uniform ground-state density

A further improvement of the accuracy can be achieved by going beyond the approximation of the tilt (17) of the spin up and down densities and, at the same time, taking into account the spatial variations of the ground-state electron density. The latter consideration is crucial since in the spill-out region the density falls rapidly to zero (see inset of Fig. 2), such that the kinetic energy contribution $E_{K,G}$ of (A2), which includes the gradients of the electronic densities, becomes important.

In this section, we assume that the magnetization profile of the surface paramagnon is given by the static magnetization induced by a static external dipolar magnetic field. Expressing the energy functional of Eq. A1 in terms of the charge and magnetization densities, the ground-state conditions for $n_0(\mathbf{r})$ and $m_0(\mathbf{r})$ are

$$\left. \frac{\delta E[n, m]}{\delta n(\mathbf{r})} \right|_{n=n_0(\mathbf{r})} = \left. \frac{\delta E[n, m]}{\delta m(\mathbf{r})} \right|_{m=m_0(\mathbf{r})} = 0. \quad (21)$$

Applying an external magnetic field along the z axis, $\mathbf{B}_{\text{ex}}(\mathbf{r}) = B_{\text{ex}}(\mathbf{r})\hat{\mathbf{z}}$ results (with $g\mu_B = 1$ in atomic units and the negative charge of the electron) in an additional contribution to the total energy functional

$$E_T[n, m] = E[n, m] + \int d\mathbf{r} B_{\text{ex}}(\mathbf{r}) m(\mathbf{r}). \quad (22)$$

If we work with a spherically symmetric nanoparticle, the charge and spin channels are decoupled. Thus, in linear response, the application of a magnetic field does not affect $n_0(\mathbf{r})$, and we drop this functional variable hereafter. The magnetization density is driven from

its ground-state value $m_0(\mathbf{r}) = 0$ to a perturbed value $\Delta m(\mathbf{r})$, which is given by

$$\left. \frac{\delta E[m]}{\delta m(\mathbf{r})} \right|_{m=\Delta m(\mathbf{r})} = -B_{\text{ex}}(\mathbf{r}). \quad (23)$$

Once the applied field is removed, the nanoparticle is left with an extra-energy

$$\begin{aligned} \Delta E &\simeq \frac{1}{2} \int d\mathbf{r} \int d\mathbf{r}' \left. \frac{\delta^2 E[m]}{\delta m(\mathbf{r}) \delta m(\mathbf{r}')} \right|_{m=m_0} \Delta m(\mathbf{r}) \Delta m(\mathbf{r}') \\ &= \frac{1}{2} \int d\mathbf{r} B_{\text{in}}(\mathbf{r}) \Delta m(\mathbf{r}). \end{aligned} \quad (24)$$

In the last equality we have used the perturbed equilibrium condition (23) and defined $B_{\text{in}} = -B_{\text{ex}}$ as an internal field that counterbalances the applied one. Once the perturbation is switched off, the dynamics of the magnetization is determined by the excess energy ΔE .

For the dipolar excitations that we are interested in (*i.e.* Eq. 12b) an appropriate choice for the external field is $B_{\text{ex}} = -z/\lambda_B$, with $1/\lambda_B$ measuring the strength of the perturbation. With (15), this allows us to write the extra energy as

$$\Delta E = \frac{1}{2\lambda_B} \int d\mathbf{r} z \Delta m(\mathbf{r}) = \frac{NZ^\dagger}{2\lambda_B}. \quad (25)$$

The condition (23) and the form of B_{ex} fix the induced magnetization, which we can write as $\Delta m(\mathbf{r}) = \delta m_R(r) \cos \theta$. Defining the quantity $\tilde{m}(r) = \lambda_B r^2 \delta m_R(r)$, we show in App. B that in the linear régime the magnetization profile is determined by the differential equation

$$-D(r) \tilde{m}'(r) + \left[D(r) \left(\frac{2}{r} + 36D(r) \right) + A_{\text{KS}}(r) \right] \tilde{m}(r) = n_0(r)r^3, \quad (26)$$

where

$$A_{\text{KS}}(r) = \left(\frac{1}{12\pi^2} \right)^{1/3} \frac{1}{r_s(r)} \left[\left(\frac{3\pi^2}{2} \right)^{2/3} \frac{1}{r_s(r)} - 1 + c(r_s(r)) \right], \quad (27a)$$

$$D(r) = \frac{1}{36} \frac{n'_0(r)}{n_0(r)}, \quad (27b)$$

with $n_0(r)$ being the electron density in the ground state which can be calculated numerically from a static LSDA code. The primes denote derivatives with respect to r .

As in the simpler case of a tilt-like magnetization, we assume that the functional form of the magnetization profile is conserved, up to an overall factor, in the oscillations occurring when the external field is switched off. Such an assumption is supported by the numerical

results shown in Fig. 3. The magnetization profile obtained at resonance ($\omega = \omega_{\text{sd}}$, filled circles, right scale) is much stronger but very close in shape to the static one ($\omega = 0$, $B_{\text{ex}} = -z/\lambda_B$, empty circles, left scale). It is important to notice that the solution $\tilde{m}(r)$ of Eq. 26 (thin solid line) is a good representation of the local spin-density calculations. The differences for small values of r are not significant because of the volume integrals that

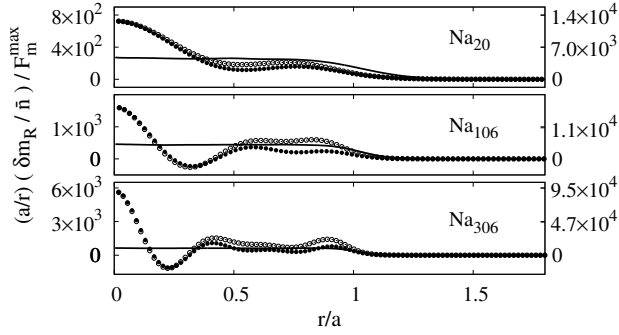


FIG. 3: Radial part of the magnetization profile for various particle sizes. The filled circles represent the TDLSDA calculations near the frequency of the surface paramagnon (right scale). The empty circles are the static results obtained from LSDA with an external field $B_{\text{ex}} = -z/\lambda_B$ (left scale). The solid line is the solution of (26) based on a non-uniform ground-state electron density. The normalization of the magnetization profile differs from that of Fig. 1 by a factor $(r/a)^3$, such that the tilted spin densities (17) result in a step function.

are performed. In addition, we see from Fig. 3 that the various approximations for the magnetization profile do not deviate considerably from the simple tilt (17) that we used in the previous chapter. Even if the magnetization profile attains its maximum value around $r = a$, the spin dipole is not a surface mode (in contrast to the surface plasmon), since the excitation is not confined to the surface but appears in the whole nanoparticle.

The restoring force associated with ΔE , Eq. 25, leads to oscillations of the two spin populations with a frequency

$$\hat{\omega}_S = \sqrt{\frac{2 \Delta E}{N Z^{\dagger 2}}} = \sqrt{\frac{3}{4\pi} \frac{N}{\int dr r \tilde{m}(r)}}. \quad (28)$$

Using the profile $\tilde{m}(r)$ from (26) we obtain a good approximation (pluses in Fig. 2) of the numerically obtained ω_{sd} . This shows the importance of the spill-out in determining the frequency of the spin-dipole excitations, and underlines that the corresponding shift can be accurately estimated from the equilibrium density profiles²⁵.

IV. SPIN-DIPOLE SPECTRUM AND PARTICLE-HOLE EXCITATIONS

In the preceding section, we have identified the behavior of the lowest frequency peak in the spin-dipole absorption spectrum. Two important questions deserve to be addressed now. The first concerns the specificity of the lowest energy peak as compared with the other ones. The second question, already treated in the literature⁸, partly in the context of electronic excitations in quantum dots¹⁷, is whether or not the spin dipole can be consid-

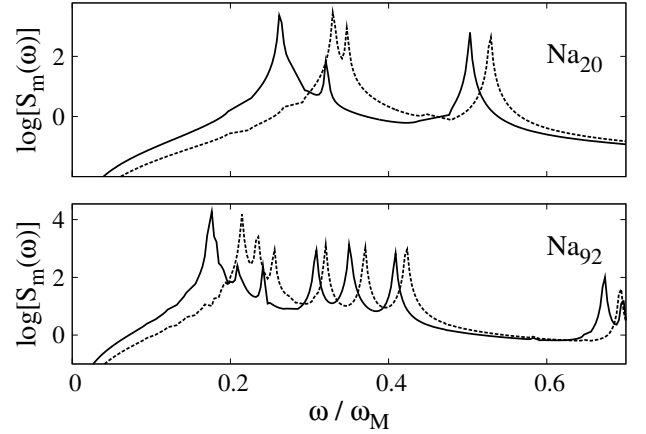


FIG. 4: Spin-dipole absorption spectrum (solid line) and particle-hole excitation spectrum (dashed line) for two nanoparticle sizes.

ered to be a collective excitation, as it is the case for the surface plasmon.

In Fig. 1 we saw that in addition to its considerably larger oscillator strength, the first peak is peculiar from the point of view of the induced magnetization which has significant contributions of constant sign, whereas there are always important contributions of different sign for the other peaks. The assumption of a tilt for the magnetization profile used in our analytical approach of Sec. III A is appropriate to describe a mode without nodes and thus allows for an estimate of the frequency of the lowest peak. In the semi-analytical model of Sec. III B, the magnetization is supposed to be generated by an external magnetic field that is linear in z . The radial components of the magnetization profiles obtained numerically are also positive except for a very small insignificant region close to the center in the largest particles (see Fig. 3). In order to predict the frequencies of higher-energy peaks in the spectrum, one would have to assume more complex magnetization profiles. However, those peaks show no obvious regularities in their magnetization profile (*e.g.* the number of nodes does not increase monotonically when moving to higher frequencies). One can conclude that the first peak really stands out as the only one with an essentially everywhere-positive magnetization, a property that allowed us to construct a rather precise theory for the frequency associated with this mode.

The authors of Ref. 8 concluded that the surface paramagnon is a collective excitation, based on the observation that the resonance exhausts more than 90 % of the total spectral weight. A widely accepted criterion is to consider an excitation as collective if it results from the superposition of a large number of low-energy particle-hole excitations. This is certainly the case of the well-studied surface plasmon^{26,27}, where the residual interaction (understood in this context as going beyond the Hartree-Fock approximation) results in a small perturba-

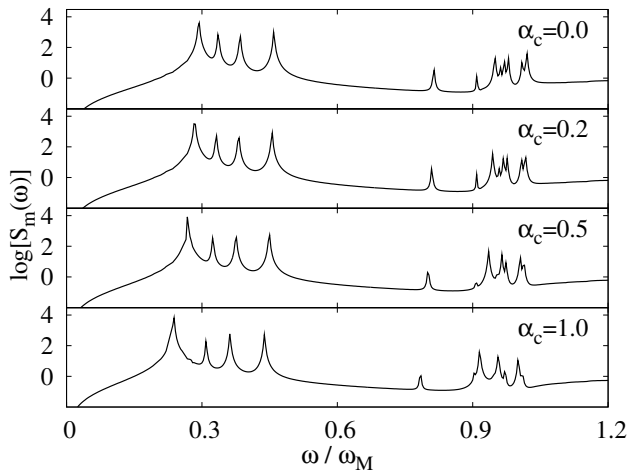


FIG. 5: Spin-dipole absorption spectrum for Na_{34} and increasing values of α_c corresponding to an increasing importance of the interactions.

tion of most of the particle-hole excitations and the appearance of the collective excitation in the high-energy sector of the spectrum. The considerably lower energy of the spin dipole and its size scaling suggest some important differences in the nature of the two excitations. In order to test this conjecture, we show in Fig. 4 a comparison between the full spin-dipole absorption spectrum (solid lines) and the corresponding particle-hole excitation spectrum (dashed). The latter is obtained by removing the electron-electron interaction in the calculation of the linear response (setting $\alpha_c = 0$ in Eq. 7), although it is still included when computing the ground state. Since there is no Hartree contribution for the spin modes, the residual interaction in this context is understood as the effective exchange-correlation term (8). We can see that the two spectra have similar structure, with a one-to-one correspondence between the excitations. The full spin-dipole absorption spectrum appears to be slightly red-shifted as compared to the particle-hole spectrum because of the attractive nature of the exchange-correlation interaction.

The selection rules for dipole-created electron-hole excitations dictate a minimal absorption energy²⁷, associated with a frequency $\omega_{\text{ph}}^{\text{min}} \simeq (\pi/2)(9\pi/4)^{1/3}N^{-1/3}\bar{r}_s^{-2}$ which has the observed size scaling of ω_{sd} . This estimation of the first peak of the non-interacting absorption spectrum (dashed lines in Fig. 4) agrees within 20 % with the frequency that is obtained from Eq. 20 by only keeping the one-body (kinetic energy) component. Once we consider exchange and correlation corrections, the previous excitation splits according to its total spin. The spin selection rules tell us that the lower frequency appears in the absorption spectrum (solid lines in Fig. 4). The corresponding shift can in principle be extracted within the local density functional approximation provided the single-particle wave-functions are known.

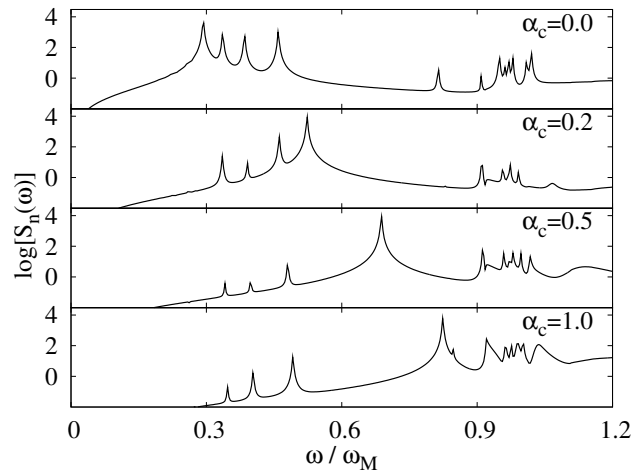


FIG. 6: Charge dipole absorption spectrum for Na_{34} and different values of α_c . For $\alpha_c = 1$, the surface plasmon frequency $\omega_{\text{sp}} \simeq 0.8\omega_M$ is recovered.

In order to investigate in more detail the evolution of the single-particle excitations into spin modes we vary α_c in Eq. 7 from the noninteracting particle-hole case $\alpha_c = 0$ to full spin-dipole excitation $\alpha_c = 1$. Fig. 5 shows the evolution of the spin-dipole absorption spectrum with α_c for Na_{34} . One can see that the structure of the spectrum is not modified by the interaction strength. The lowest-frequency peak is always the dominating one, and its strength is hardly changed. The whole spectrum is red-shifted by the interaction, which is globally attractive in this case.

The behavior of the spin dipole can be contrasted with that of the charge dipole (Fig. 6). When $\alpha_c = 0$, the four particle-hole excitation modes previously obtained can be observed at frequencies lower than $0.5\omega_M \approx 1.7\text{ eV}$. By gradually increasing α_c , three of the modes are slightly blue-shifted and become considerably weaker, while the fourth one experiences a much larger blue shift and dominates the other peaks for $\alpha_c > 0.2$, eventually by several orders of magnitude. For $\alpha_c = 1$, this peak coincides with the surface plasmon, which is a collective excitation with $\omega_{\text{sp}} \simeq 2.8\text{ eV} \approx 0.8\omega_M$.

These findings are at odds with the claims of Serra *et al.*⁸, who interpreted the surface paramagnon as a collective excitation. In contrast, our results indicate that the various spin-dipole modes appearing in the absorption spectrum should be viewed as individual particle-hole excitations, slightly modified by the electron-electron interaction.

V. OPEN-SHELL SYSTEMS

For closed-shell systems, an electric dipole field only couples to the charge dipole in the linear regime and the excitation of the surface plasmon dominates the absorp-

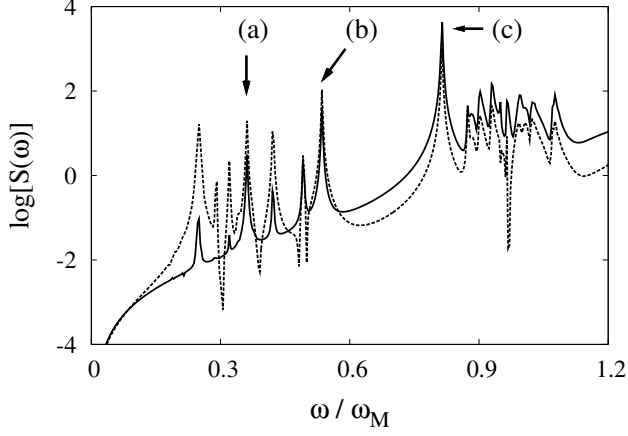


FIG. 7: Dipole absorption spectrum S_n (solid line) and dipole-induced spin-dipole absorption spectrum S_{mn} (dashed line) for Na_{27} . The frequencies of peaks (a), (b), and (c) are 1.22, 1.82, and 2.77 eV, respectively.

tion of laser light. One possibility to observe cross-talking between the charge and dipole modes is to operate in the nonlinear regime with strong excitations¹⁰. This may raise some practical difficulties, such as electrons escaping the nanoparticle, thus leaving behind a net positive charge. Another possibility is to work with open-shell systems that possess an intrinsic magnetization in the ground state, so that the charge and spin modes are coupled even in the linear regime^{12,17}.

In Fig. 7, we show the dipole absorption spectrum S_n and dipole-induced spin-dipole absorption spectrum S_{mn} for a Na_{27} nanoparticle²⁸. In both cases, the system is excited by an oscillating electric field which induces both a charge-dipole mode (solid curve) and a spin-dipole mode (dotted curve). The charge and magnetization profiles corresponding to some of the observed peaks are plotted in Fig. 8.

The strongest coupling between the charge and spin channels occurs at the frequency of the surface plasmon. For high-energy peaks, the charge-dipole response dominates its spin-dipole counterpart, while the spin-dipole response is more important in the low-energy spectrum. The peak labeled (b) in Fig. 7 appears as a special case – with an energy intermediate between that of the surface paramagnon and surface plasmon modes – for which the spin-dipole response is comparable to the charge-dipole response. The same qualitative features have been observed in the spectra of other open-shell systems.

In the sequel we focus on the maximum of the spin-dipole response that occurs at the surface plasmon frequency for systems with non-zero ground state magnetization (peak (c) in Fig. 7). For weak excitations, the dynamical magnetization can be written as

$$\Delta m(\mathbf{r}) = \Delta \xi(\mathbf{r}) n_0(\mathbf{r}) + \Delta n(\mathbf{r}) \xi_0(\mathbf{r}) \quad (29)$$

in terms of the ground-state electron density $n_0(\mathbf{r})$, the ground-state polarization $\xi_0(\mathbf{r})$, and their dynamical counterparts $\Delta n(\mathbf{r})$ and $\Delta \xi(\mathbf{r})$.

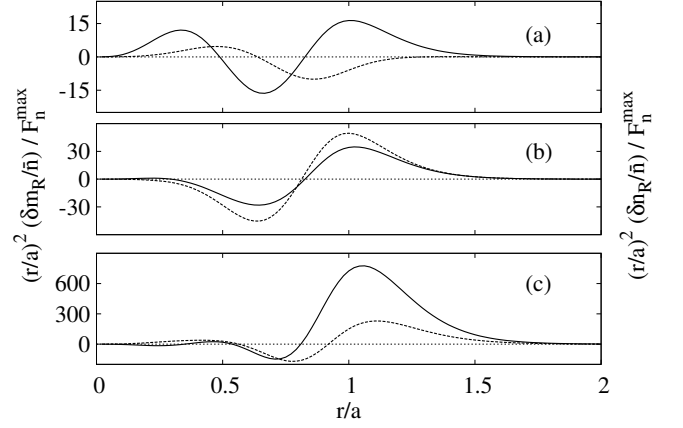


FIG. 8: Radial part of the dynamical charge (solid lines) and magnetization densities (dashed lines) corresponding to the peaks highlighted in Fig. 7. The normalizations are as in Fig. 1.

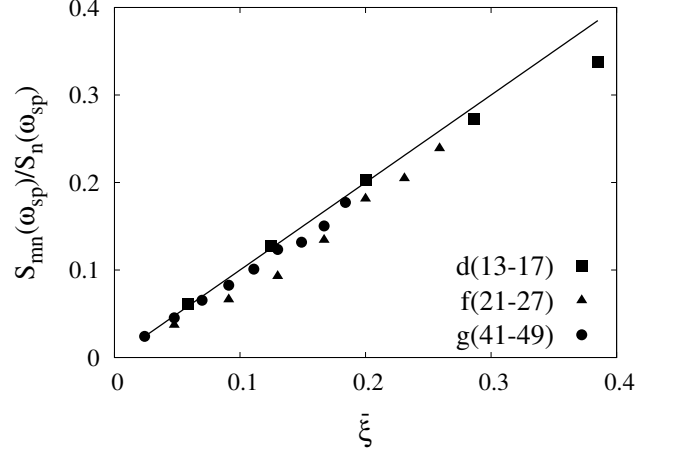


FIG. 9: Ratio of the spin-dipole to charge-dipole absorption cross-section for a spin-independent excitation at the surface plasmon frequency, as a function of the mean ground-state spin polarization ξ . Squares refer to particles $\text{Na}_{13} - \text{Na}_{17}$, triangles to particles $\text{Na}_{21} - \text{Na}_{27}$, and dots to particles $\text{Na}_{41} - \text{Na}_{49}$, where the open electronic shells are d, f, and g, respectively.

cal counterparts $\Delta n(\mathbf{r})$ and $\Delta \xi(\mathbf{r})$. As the laser light couples essentially to the charge degrees of freedom, the excitation has the form of a shift Z of the entire electron population. The dynamical excitation density is thus concentrated at the surface and, in the hard-wall homogeneous density approximation, given by $\Delta n(\mathbf{r}) = \bar{n} Z \delta(a - r) \cos \theta$, just like in the case of the surface plasmon. The resulting charge excitation corresponds to a peak at the surface plasmon frequency ω_{sp} in the absorption spectrum of Fig. 7.

In addition, even though the excitation does not act directly on the spin polarization (*i.e.* $\Delta \xi(\mathbf{r}) = 0$), the dynamical magnetization corresponding to the charge dis-

placement $\Delta m(\mathbf{r}) = \Delta n(\mathbf{r})\xi_0(\mathbf{r})$ does not vanish when $\xi_0 \neq 0$. Assuming that the polarization $\xi_0(\mathbf{r})$ is uniform inside the particle, and equal to the mean spin polarization $\bar{\xi} = (N^\uparrow - N^\downarrow)/N$ (for the example of Na_{27} ²⁸ one has $\bar{\xi} = 7/27 \approx 0.26$), we obtain a response to the spin-independent excitation $V_{\text{ex},n}$ in the magnetization channel $\Delta m(\mathbf{r})$ which is proportional to the induced $\Delta n(\mathbf{r})$ in the charge channel, with proportionality constant $\bar{\xi}$. Therefore, we expect

$$S_{mn}(\omega_{\text{sp}}) = \bar{\xi} S_n(\omega_{\text{sp}}). \quad (30)$$

In Fig. 9 we present results of TDLSDA calculations with spin-independent excitation for the mode with $\omega = \omega_{\text{sp}}$, for a variety of open-shell nanoparticles. The ratio between the spin-dipole and charge-dipole absorption cross-sections for not too large polarization is indeed to a very good approximation given by the mean ground-state polarization $\bar{\xi}$. This allows us to predict particularly strong cross-talk between the spin-dipole and the surface plasmon modes for open-shell nanoparticles having large ground-state polarizations.

VI. CONCLUSION

In this work, we have studied the spin-dependent linear response in alkali-metal (particularly sodium) nanoparticles. Our primary aim was to achieve some insight into the nature of these modes, which were first investigated by Serra and collaborators^{8,9}. Towards this goal we derived simple analytical and semi-analytical models that were confronted with linear response TDLSDA calculations.

The spin-dipole absorption spectrum displays a number of peaks at frequencies lower than the surface plasmon frequency. The lowest of them is characterized by a magnetization profile without nodes. An excess of spin-up electrons is built in half of the nanoparticle at the expense of the spin-down electrons, which are majority in the other half of the nanoparticle. The restoring force of such a non-equilibrium configuration results in the out-of-phase oscillation of the two spin subsystems. The local spin-density approximation can be used to estimate the restoring force, and within a classical picture, we could estimate the lowest frequency. This approach provides the correct scaling of the frequency with the particle size (as $N^{-1/3}$), albeit blue-shifted with respect to the TDLSDA results. Such a deviation is partially corrected by including the spill-out effect in a phenomenological way using the numerically obtained surface plasmon frequencies instead of the Mie value. A more sophisticated model, taking into account the inhomogeneities in the ground-state density and gradient corrections, yielded an even better agreement.

By comparing the spin-dipole absorption spectrum with that obtained by progressively removing the electron-electron interaction, we observed a one-to-one correspondence of the particle-hole excitations and the

spin-dipole modes. We thus showed that the spin-dipole modes are slight perturbations of the particle-hole excitations, and therefore do not qualify as genuine collective excitations, contrary to the claim of Ref. 8.

Finally, we studied the possibility of exciting the spin-dipole modes by ordinary optical means (laser pulses). For open-shell systems, it is well-known that the spin and charge modes are coupled in the linear regime^{12,17}. We showed that, when exciting the system with a density shift, a spin-dipole mode appears at the surface plasmon frequency, together with the standard charge-dipole mode. The ratio between the strengths of the absorption peak for the spin dipole and charge dipole modes was shown to be given by the spin polarization of the ground-state.

While our numerical calculations were done in the case of Na nanoparticles, our general conclusions are also valid for noble-metal nanoparticles and semiconductor quantum dots. The latter systems are more adapted than alkaline nanoparticles for experimental spectroscopic studies. Moreover, the concepts developed for the study of spin modes in normal-metal nanoparticles could be useful in analyzing ferromagnetic nanoparticles, in view of the strong internal field existing in these materials.

Acknowledgments

We thank M. Barranco for helpful correspondence and we acknowledge financial support from the French National Research Agency ANR (project ANR-06-BLAN-0059).

APPENDIX A: LSDA PARAMETRIZATION

Our numerical and analytical approaches to obtain the spin-dipole resonances are based on the local spin density approximation¹⁶. For completeness we present in this appendix the particular parametrization that we chose in our approaches. The energy functional of the electron system can be written as

$$E[n^\uparrow, n^\downarrow] = E_K[n^\uparrow, n^\downarrow] + E_H[n] + E_{\text{XC}}[n^\uparrow, n^\downarrow], \quad (\text{A1})$$

where E_K represents the kinetic energy, E_H the Hartree contribution, and E_{XC} the exchange-correlation term. The kinetic energy is given by

$$E_K[n^\uparrow, n^\downarrow] = E_{\text{K,TF}}[n^\uparrow, n^\downarrow] + E_{\text{K,G}}[n^\uparrow, n^\downarrow], \quad (\text{A2})$$

with the Thomas-Fermi component

$$E_{\text{K,TF}}[n^\uparrow, n^\downarrow] = \frac{3}{10} (6\pi^2)^{2/3} \int d\mathbf{r} \left(n^{\uparrow 5/3}(\mathbf{r}) + n^{\downarrow 5/3}(\mathbf{r}) \right) \quad (\text{A3})$$

and the gradient correction

$$E_{\text{K,G}}[n^\uparrow, n^\downarrow] = \frac{1}{72} \int d\mathbf{r} \left(\frac{|\nabla n^\uparrow|^2}{n^\uparrow} + \frac{|\nabla n^\downarrow|^2}{n^\downarrow} \right), \quad (\text{A4})$$

which takes into account the spatial density variations in the electron gas^{3,29}. This term is particularly relevant when we consider spill-out effects and thus a finite region where the density exhibits large spatial variations (as in Sec. IIIB).

The Hartree contribution depends only on the total density $n = n^\uparrow + n^\downarrow$, and is given by the electrostatic potential energy

$$E_H[n^\uparrow, n^\downarrow] = \frac{1}{2} \iint d\mathbf{r} d\mathbf{r}' \frac{n(\mathbf{r})n(\mathbf{r}')}{|\mathbf{r} - \mathbf{r}'|}. \quad (\text{A5})$$

This term is irrelevant for spin-dipole excitations in spherically symmetric nanoparticles since they do not involve charge displacements.

The exchange-correlation term can be expressed in terms of the exchange and correlation components as $E_{XC} = E_X + E_C$ with

$$E_{X/C}[n^\uparrow, n^\downarrow] = \int d\mathbf{r} n(\mathbf{r}) \epsilon_{X/C}(n^\uparrow, n^\downarrow). \quad (\text{A6})$$

The function $\epsilon_{xc} = \epsilon_x + \epsilon_c$ determines the exchange-correlation potential through Eq. 5. For the exchange part one has

$$\epsilon_x(n^\uparrow, n^\downarrow) = -\frac{3}{2} \left(\frac{3}{4\pi} \right)^{1/3} \left(n^{\uparrow 4/3} + n^{\downarrow 4/3} \right) / n. \quad (\text{A7})$$

For ϵ_c we use²¹

$$\epsilon_c(n^\uparrow, n^\downarrow) = \epsilon_c^U(r_s) + [\epsilon_c^P(r_s) - \epsilon_c^U(r_s)] f(\xi) \quad (\text{A8})$$

with

$$\epsilon_c^U(r_s) = \frac{-0.1423}{1 + 1.0529\sqrt{r_s} + 0.3334 r_s} \quad (\text{A9})$$

$$\epsilon_c^P(r_s) = \frac{-0.0843}{1 + 1.3981\sqrt{r_s} + 0.2611 r_s} \quad (\text{A10})$$

$$f(\xi) = \frac{(1 + \xi)^{4/3} + (1 - \xi)^{4/3} - 2}{2^{4/3} - 2}. \quad (\text{A11})$$

The normalized inter-particle distance $r_s = (4\pi n/3)^{-1/3}$ and the spin polarization $\xi = (n^\uparrow - n^\downarrow)/n$ are both local properties of the electron system. The above parametrization of E_{XC} was used in our analytical approaches, as well as in the numerics, since it has been proven to provide a good representation for the electron densities that we are interested in.

APPENDIX B: MAGNETIZATION PROFILE FOR NON-UNIFORM GROUND-STATE DENSITIES

In this appendix we develop the perturbed equilibrium condition (23) for a closed-shell nanoparticle in an external magnetic field and derive the differential equation (26) for the magnetization profile.

Expressing Eq. 23 in terms of the polarization we have

$$\frac{1}{n_0(r)} \frac{\delta E[\xi]}{\delta \xi(\mathbf{r})} \Big|_{\xi=\Delta\xi(\mathbf{r})} = \frac{z}{\lambda_B}. \quad (\text{B1})$$

Similarly as in (18), we can write the functional derivatives of $E_{K,TF}$, E_X , and E_C , respectively, as

$$\frac{1}{n_0(r)} \frac{\delta E_{K,TF}}{\delta \xi(\mathbf{r})} = \frac{(3\pi^2)^{2/3}}{4} n_0^{2/3}(r) \left([1 + \xi(\mathbf{r})]^{2/3} - [1 - \xi(\mathbf{r})]^{2/3} \right), \quad (\text{B2a})$$

$$\frac{1}{n_0(r)} \frac{\delta E_X}{\delta \xi(\mathbf{r})} = -\frac{1}{2} \left(\frac{3}{\pi} \right)^{1/3} n_0^{1/3}(r) \left([1 + \xi(\mathbf{r})]^{1/3} - [1 - \xi(\mathbf{r})]^{1/3} \right), \quad (\text{B2b})$$

$$\frac{1}{n_0(r)} \frac{\delta E_C}{\delta \xi(\mathbf{r})} = [\epsilon_c^P(r_s(r)) - \epsilon_c^U(r_s(r))] f'(\xi(\mathbf{r})), \quad (\text{B2c})$$

where f' stands for the derivative of the function f defined in (A11). Because of large density variations in the spill-out region we consider the gradient correction (A4) for which we get

$$\frac{1}{n_0(r)} \frac{\delta E_{K,G}}{\delta \xi(\mathbf{r})} = \frac{1}{72n_0(r)} \frac{\delta}{\delta \xi(\mathbf{r})} \left\{ \int d\mathbf{r} \left(\frac{|\nabla n_0|^2}{n_0(r)} + n_0(r) \frac{|\nabla \xi(\mathbf{r})|^2}{1 - \xi^2(\mathbf{r})} \right) \right\}. \quad (\text{B3})$$

The first term of the integrand is independent of $\xi(\mathbf{r})$, and the second can be treated using partial integration yielding

$$\frac{1}{n_0(r)} \frac{\delta E_{K,G}}{\delta \xi(\mathbf{r})} = \frac{1}{36} \left(\frac{\xi(\mathbf{r}) |\nabla \xi(\mathbf{r})|^2}{[1 - \xi^2(\mathbf{r})]^2} - \frac{1}{n_0(r)} \nabla \left(\frac{n_0(r) \nabla \xi(\mathbf{r})}{1 - \xi^2(\mathbf{r})} \right) \right). \quad (\text{B4})$$

Since $\nabla n_0(r) = n'_0(r) \hat{\mathbf{r}}$, we have $\nabla(n_0(r) \nabla \xi(\mathbf{r})) = n'_0(r) (\partial \xi(\mathbf{r}) / \partial r) + n_0(r) \nabla^2 \xi(\mathbf{r})$. Assuming that the polarization is small and a smooth function of \mathbf{r} verifying $\nabla^2 \xi \ll \partial \xi(\mathbf{r}) / \partial r$ we remain in linear order in ξ and write

$$\frac{1}{n_0(r)} \frac{\delta E_{K,G}}{\delta \xi(\mathbf{r})} \approx -\frac{1}{36} \frac{n'_0(r)}{n_0(r)} \frac{\partial \xi(\mathbf{r})}{\partial r}. \quad (\text{B5})$$

Gathering the various contributions to the energy, Eq. B1 becomes

$$-\frac{1}{36} \frac{n'_0(r)}{n_0(r)} \frac{\partial \Delta \xi(\mathbf{r})}{\partial r} + A_{KS} \xi(\mathbf{r}) = \frac{r}{\lambda_B} \cos \theta, \quad (\text{B6})$$

with A_{KS} defined in (27a). Since Eq. B6 admits solutions of the dipolar form, we write $\Delta \xi(\mathbf{r}) = \delta \xi_R(r) \cos \theta$ and $\tilde{m}(r) = \lambda_B r^2 n(r) \delta \xi_R(r)$, obtaining Eq. 26 for the magnetization profile. The function $\tilde{m}(r)$ is more appropriate than $\delta \xi_R(r)$ for numerical calculations dealing with small electron densities.

-
- ¹ U. Kreibitz and M. Vollmer, *Optical Properties of Metal Clusters* (Springer, Berlin, 1995).
 - ² W. A. de Heer, Rev. Mod. Phys. **65**, 611 (1993).
 - ³ M. Brack, Rev. Mod. Phys. **65**, 677 (1993).
 - ⁴ C. Br  chignac, Ph. Cahuzac, N. Keb  ili, J. Leygnier, and A. Sarfati, Phys. Rev. Lett. **68**, 3916 (1992); C. Br  chignac, Ph. Cahuzac, J. Leygnier, and A. Sarfati, Phys. Rev. Lett. **70**, 2036 (1993).
 - ⁵ J.-Y. Bigot, J.-C. Merle, O. Cregut, and A. Daunois, Phys. Rev. Lett. **75** 4702 (1995); J.-Y. Bigot, V. Halt  , J.-C. Merle, and A. Daunois, Chem. Phys. **251**, 181 (2000).
 - ⁶ C.-K. Sun, F. Vall  e, L. H. Acioli, E. P. Ippen, and J. G. Fujimoto, Phys. Rev. B **50**, 15337 (1994).
 - ⁷ L. H. F. Andrade, A. Laraoui, M. Vomir, D. Muller, J.-P. Stoquert, C. Estourn  s, E. Beaupaire, and J.-Y. Bigot, Phys. Rev. Lett. **97**, 127401 (2007).
 - ⁸ L. Serra, R. A. Broglia, M. Barranco, J. Navarro, Phys. Rev. A **47**, R1601 (1993).
 - ⁹ L. Serra and E. Lipparini, Europhys. Lett. **40**, 667 (1997).
 - ¹⁰ L. Mornas, F. Calvayrac, E. Suraud, and P.-G. Reinhard, Z. Phys. D **38**, 73 (1996).
 - ¹¹ C. Kohl, S. M. El Gammal, F. Calvayrac, E. Suraud, and P.-G. Reinhard, Eur. Phys. J. D **5**, 271 (1999).
 - ¹² M. B. Torres and L. L. Balb  s, J. Phys.: Condens. Matter **12**, 4365 (2000).
 - ¹³ P.-G. Reinhard, V. O. Nesterenko, E. Suraud, S. El Gammal, and W. Kleinig, Phys. Rev. A **66**, 013206 (2002).
 - ¹⁴ A. Pinczuk and G. Abstreiter, in *Light Scattering in Solids V*, Topics in Applied Physics **66**, ed. by M. Cardona and G. G  ntherodt, Springer-Verlag (Berlin and Heidelberg, 1989).
 - ¹⁵ C. Sch  ller, K. Keller, G. Biese, E. Ulrichs, L. Rolf, C. Steinebach, and D. Heitmann, Phys. Rev. Lett. **80**, 2673 (1998).
 - ¹⁶ E. Lipparini, *Modern Many-Particle Physics: Atomic Gases, Quantum Dots and Quantum Fluids*, World Scientific (Singapore 2003).
 - ¹⁷ Ll. Serra, M. Barranco, A. Emperador, M. Pi, and E. Lipparini, Phys. Rev. B **59**, 15290 (1999).
 - ¹⁸ L. Colletti, F. Pederiva, E. Lipparini, and C. J. Umrigar, Phys. stat. sol. (b) **244**, 2317 (2007).
 - ¹⁹ A. Puente, M. Casas, and Ll. Serra, Physica E **8**, 387 (2000).
 - ²⁰ A. K. Rajagopal, Phys. Rev. B **17** 2980 (1978).
 - ²¹ J. P. Perdew and A. Zunger, Phys. Rev. B **23**, 5048 (1981).
 - ²² The electron configuration of Na₃₄ can be expressed as $1s^2 1p^6 1d^{10} 2s^2 1f^{14}$.
 - ²³ E. Lipparini and M. Califano, Z. Phys. D **37**, 365 (1996).
 - ²⁴ G. Weick, G.-L. Ingold, R.A. Jalabert, and D. Weinmann, Phys. Rev. B **74**, 165421 (2006).
 - ²⁵ Following similar lines in the case of a charge-dipole excitation we obtain for the surface plasmon frequency the estimation $\tilde{\omega}_M^2 = (3N/4\pi)(\int dr r \tilde{n}(r))^{-1}$, where $\tilde{n}(r) = \lambda_E r^2 \delta n_R(r)$ with $\delta n_R(r)$ being the radial part of the density perturbation and λ_E giving the strength of the perturbing field. Analogously to Eq. 26, \tilde{n} verifies an integro-differential equation involving a Hartree term, as well as the other contributions to the energy (A1).
 - ²⁶ C. Yannouleas and R. A. Broglia, Ann. Phys. (N. Y.) **217**, 105 (1992).
 - ²⁷ C. Seoanez, G. Weick, R. A. Jalabert, and D. Weinmann, Eur. Phys. J. D **44**, 351 (2007).
 - ²⁸ The electron configuration of Na₂₇ can be expressed as $1s^2 1p^6 1d^{10} 2s^2 1f^7$. According to Hund's rule, the spins of the 7 *f*-electrons are aligned.
 - ²⁹ G. L. Oliver and J. P. Perdew, Phys. Rev. A **20**, 397 (1979).